Thermal Design Procedure for Micro- and Nano-satellites Pointing to Earth

Tsuyoshi Totani,[1] Hiroto Ogawa,[2] Ryota Inoue,[3] Tilok K. Das,[4] Masashi Wakita[5] and Harunori Nagata[6]

Hokkaido University, Sapporo, Hokkaido, 060-8628, Japan

This paper proposes a thermal design procedure for micro- and nano-satellites that can be completed in 1 year. Two thermal design concepts keep components within their design temperature range: reducing the temperature change by using the whole structure for heat storage and reducing the temperature change of the inner structure where the most temperature-sensitive components are mounted. One- and two-nodal analysis methods are used for the former and latter concepts, respectively, to clarify the combinations of optical properties for the structures and components to keep within the design temperature range of the components. Finally, multi-nodal analysis is performed for detail design based on the optical properties clarified from the one- and two-nodal analyses. This thermal design procedure was applied to the Hodoyoshi-1 satellite, which is a cube about 50 cm on a side, has two inner plates and has solar cells on the body, is on a Sun-synchronous orbit at an altitude of about 500 km, and is pointing to Earth. The thermal design of the Hodoyoshi-1 satellite was completed in about ten months.

Nomenclature

a = albedo factor

A_i = area including node i

[1] Associate Professor, Faculty of Engineering, Kita 13, Nishi 8, and Senior Member.
[2] Graduate Student, Graduate School of Engineering, Kita 13, Nishi 8, and Non-member.
[3] Graduate Student, Graduate School of Engineering, Kita 13, Nishi 8, and Non-member.
[4] Graduate Student, Graduate School of Engineering, Kita 13, Nishi 8, and Non-member.
[5] Assistant Professor, Faculty of Engineering, Kita 13, Nishi 8, and Member.
[6] Professor, Faculty of Engineering, Kita 13, Nishi 8 , and Member.

$A_{p/l}$ = projected unit area with respect to Sun

A_{sp} = area of spacer inserted between inner structure and outer structure

c_i = specific heat

F = configuration factor

F_a = configuration factor in case of albedo

$F_{i\text{-}j}$ = configuration factor from node i to node j

$F_{s\text{-}e}$ = configuration factor from satellite to Earth

G_s = solar constant

H = altitude

k = conductivity

l = length of one side of satellite

L = thickness of spacer inserted between inner structure and outer structure

m_i = mass of node i

P = period of orbit

P_{gen} = generation power at solar cell

q_{IR} = Earth infrared radiation

$\dot{Q}_{ex}$ = net heat rate of absorbed input heat

$\dot{Q}_i$ = heat dissipation rate at node i

$\dot{Q}_{i-j}$ = net heat transfer rate from node i to node j

$\dot{Q}_{i-j\,c}$ = net heat transfer rate of heat conduction from node i to node j

$\dot{Q}_{i-j\,r}$ = net heat transfer rate of radiation from node i to node j

$\dot{Q}_{sh\_i}$ = heat dissipation rate at shunt in node i

R_e = radius of Earth

T_i = temperature at node i

t = time

Node i and j denote inner structure node I, outer structure node O, or whole satellite node W.

Greeks

α = solar absorptivity

α_C = solar absorptivity of solar cell

α_R = solar absorptivity of radiation area on outside of outer structure

ε = infrared emissivity

ε_C = infrared emissivity of solar cell

ε_R = infrared emissivity of radiation area on outside of outer structure

η_c = power generation efficiency of solar cell

θ_{za} = zenith angle of satellite

ρ_c = area ratio of solar cell on outside of outer structure

σ = Stefan-Boltzmann constant, 5.67×10^{-8} W/(m^{2}K^4)

Subscripts

I = inner structure node

ns-e = from Earth pointing surface of satellite to Earth

O = outer structure node

O-in = inside of outer structure

O-out = outside of outer structure

ps-e = from surface parallel to position vector of satellite to Earth

W = whole satellite node

I. Introduction

In the thermal design of spacecraft, many parameters need to be determined so that the components stay in their design temperature ranges. Examples of such parameters include the absorptivities and emissivities of the outer structures, emissivities of the inner structures and components, thermal conductances between inner and outer structures and between inner structures and components, the heater power mounted on components, and the radiator area. The development of a satellite takes a long period of time; ten years is typical. This long development period has blocked the entrance of newcomers into this sector. Entrepreneurs are interested in the development of micro- and nano-satellites because of the smaller initial investment relative to normal-size satellites. The development

period of micro- and nano-satellites should be shortened to realize missions as soon as possible after an order is made. In the Establishment of New Paradigm of Space Development and Utilization with Nano-satellites Introducing Japanese-Original "Reasonably Reliable Systems Engineering" project,[1] one of the goals is for the thermal design to be completed within one year despite micro- and nano-satellites having issues with low heat capacity and power generation. A simple design is required to shorten the development period. A simple design would lead to a simple analysis, short fabrication time, and small number of test items. A thermal design procedure must be established to shorten the development period of micro- and nano-satellite. Several research groups have analyzed the temperature of micro- and nano-satellites. Weeren et al.[2] analyzed the thermal aspects of satellite downscaling and clarified that subsystems do not become thermally critical by scaling mass alone. On the other hand, there are few studies on thermal design procedures to shorten the development period of micro- and nano-satellites. This paper proposes a thermal design procedure for micro- and nano-satellites. Two simple thermal design concepts are used to keep components within the design temperature range. One- and two-nodal analyses are performed according to the simple thermal design concepts. Finally, multi-nodal analysis is carried out based on the results of the previous analyses. This thermal design procedure was applied to the Hodoyoshi-1 satellite in order to verify its validity.

II. Two Concepts for Thermal Design

Micro- and nano-satellites have masses that are less than or equal to 50 kg; they are lighter than normal-sized satellites. Thus, their temperatures change more easily because their thermal capacities are lower. Most micro- and nano-satellites have solar cells mounted on their bodies. They do not have enough electric power to control the temperature of all of their components.

The proposed thermal design procedure considers two concepts to keep components within their design temperature range: (1) reducing the change in temperature by using the entire thermal capacity of the satellite and (2) reducing the change in temperature of the inner structure where the components most sensitive to temperature are mounted. Concept 1 involves enhancing the heat transfer between components and structures and between structures by thermal conduction and radiation. Concept 2 involves insulating the heat transfer between the outer and inner structures by thermal conduction. The heat transfer between components and structures and between inner structures by thermal conduction and radiation is enhanced.

Calculating the thermal contact resistance is difficult. Ramamurthi et al.[3] reported the thermal contact conductance of molybdenum sulfide-coated joints at low temperature. Bahrami et al.[4] developed a new analytical model for the thermal contact resistance of nonconforming rough surfaces. Milanez et al.[5] presented the thermal contact conductance at low contact pressures. The thermal contact resistance changes with pressure between contact surfaces and with the surface roughness on contact surfaces. Determining the thermal contact resistance through thermal vacuum tests takes a long time. In order to decrease the influence of the thermal contact resistance, a thermal conductive sheet is inserted between components and structures and between structures. Concept 2 calls for a heat insulator between the outer and inner structures to prevent the former from conducting heat to the latter.

The structures of micro- and nano-satellites have smaller surface area than those of normal-sized satellites. Thus, the temperature difference is also smaller. Both concepts call for an aluminum alloy with high conductivity to make the temperature of the structure uniform.

III. Analysis Method

One-nodal analysis is suitable for calculating the temperature of a micro- or nano-satellite designed under concept 1. The whole satellite is considered to be one node. Two-nodal analysis, where the outer and inner structures are each considered to be one node, is adequate for concept 2. The temperature is calculated for each node. The advantage of these methods is that the parameter survey can be carried out quickly. Multi-nodal analysis is then carried out based on the results of one- and two-nodal analyses. Multi-nodal analysis can be used to calculate the temperature of the satellite in detail, but the parameter survey cannot be carried out quickly.

A. One-nodal Analysis

The energy equation in one-nodal analysis is expressed as follows:

$$m_W c_W \frac{dT_W}{dt} = \dot{Q}_{ex} - P_{gen} + \dot{Q}_W + \dot{Q}_{sh\_W} \ . \tag{1}$$

B. Two-nodal Analysis

In two-nodal analysis, the energy equation of the inner structure is

$$m_I c_I \frac{dT_I}{dt} = P_I + \dot{Q}_{sh\_I} + \dot{Q}_{O-I} \ . \tag{2}$$

The energy equation of the outer structure is

$$m_O c_O \frac{dT_O}{dt} = \dot{Q}_{ex} - P_{gen} + \dot{Q}_O + \dot{Q}_{sh\_O} + \dot{Q}_{I-O} \,. \tag{3}$$

C. Net Heat Rate of Absorbed Input Heat $\dot{Q}_{ex}$

The heat rate of the absorbed input heat is expressed as

One-nodal Analysis: $$\dot{Q}_{ex} = \alpha_{O-out} G_s A_{p/l} l^2 + \alpha_{O-out} G_s a F_a l^2 + \varepsilon_{O-out} q_{IR} F_{s-e} l^2 - \varepsilon_{O-out} 6 l^2 \sigma T_W{}^4 \,, \tag{4}$$

Two-nodal Analysis: $$\dot{Q}_{ex} = \alpha_{O-out} G_s A_{p/l} l^2 + \alpha_{O-out} G_s a F_a l^2 + \varepsilon_{O-out} q_{IR} F_{s-e} l^2 - \varepsilon_{O-out} 6 l^2 \sigma T_O{}^4 \,, \tag{5}$$

where the first term on the right hand side means the energy of direct solar radiation that is absorbed by the satellite. The second term indicates the energy of the albedo that is absorbed by the satellite. The third term is the energy of infrared radiation that is emitted from Earth's surface and absorbed by the satellite. The fourth term denotes the energy of infrared radiation from the satellite. The solar absorptivity and infrared emissivity on the outside of the outer structure are each averaged over the area:

$$\alpha_{O-out} = (1-\rho_C)\alpha_R + \rho_C \alpha_C \,, \tag{6}$$

$$\varepsilon_{O-out} = (1-\rho_C)\varepsilon_R + \rho_C \varepsilon_C \,. \tag{7}$$

The configuration factor from a satellite to Earth means the ratio of the energy reaching Earth to the energy emitted from the whole surface of the satellite. The configuration factor from the satellite to Earth is expressed for Earth-pointing satellites as[6]

$$F_{s-e} l^2 = F_{ns-e} l^2 + 4 F_{ps-e} l^2 \,, \tag{8}$$

where

$$F_{ns-e} = \left(\frac{R_e}{R_e + H} \right)^2 \,, \tag{9}$$

$$F_{ps-e}=\frac{1}{\pi}\left(\tan^{-1}\frac{1}{\sqrt{\left(\frac{R_e+H}{R_e}\right)^2-1}}-\frac{\sqrt{\left(\frac{R_e+H}{R_e}\right)^2-1}}{\left(\frac{R_e+H}{R_e}\right)^2}\right). \tag{10}$$

The Bannister approach[7] is used to calculate the configuration factor of the albedo:

$$F_a=\begin{cases}F_{s-e}\cos\theta_{za} & if\ \ \cos\theta_{za}>0\\ 0 & if\ \ \cos\theta_{za}\leq 0\end{cases}. \tag{11}$$

The projected unit area with respect to the Sun $A_{p/l}$ is calculated by vector analysis, e.g., Totani et al.'s method.[8]

D. Heat Transfer Rate between Inner and Outer Structures: $\dot{Q}_{I-O}$, $\dot{Q}_{O-I}$

The heat transfer between the inner and outer structures consists of thermal conduction and radiation. The heat transfer rates from the inner structure to the outer structure and vice versa are respectively expressed as follows:

$$\dot{Q}_{I-O}=\dot{Q}_{I-O\,r}+\dot{Q}_{I-O\,c}, \tag{12}$$

$$\dot{Q}_{O-I}=\dot{Q}_{O-I\,r}+\dot{Q}_{O-I\,c}. \tag{13}$$

The radiative heat transfer rates from the inner structure to the outer structure and vice versa are respectively expressed as follows:

$$\dot{Q}_{I-O\,r}=\sum_{enclosed\ region}\frac{\sigma\left(T_I^{\,4}-T_O^{\,4}\right)}{\left(1/\varepsilon_{O-in}-1\right)/A_O+\left(1/\varepsilon_I-1\right)/A_I+1/\left(A_I F_{I-O}\right)}, \tag{14}$$

$$\dot{Q}_{O-I\,r}=\sum_{enclosed\ region}\frac{\sigma\left(T_O^{\,4}-T_I^{\,4}\right)}{\left(1/\varepsilon_{O-in}-1\right)/A_O+\left(1/\varepsilon_I-1\right)/A_I+1/\left(A_O F_{O-I}\right)}. \tag{15}$$

The component shapes are not considered in the one- and two-nodal analyses. The configuration factors between plates are calculated as the configuration factors between the inner and outer structures in two-nodal analysis. The configuration factors between the inner and outer structures are numerically calculated using the Monte Carlo method in multi-nodal analysis. An insulator or thermal conductive sheet is inserted between the inner and outer structures. The conductive heat transfer rates from the inner structure to the outer structure and vice versa are

respectively expressed as follows:

$$\dot{Q}_{I-Oc}=kA_{sp}\frac{T_I-T_O}{L}\,, \tag{16}$$

$$\dot{Q}_{I-Oc}=kA_{sp}\frac{T_O-T_I}{L}\,. \tag{17}$$

E. Power Control Terms: P_{gen}, $\dot{Q}_{sh\_i}$, P_i

The generation and dissipation of electric power are separated into four condition: (1) eclipse, (2) less electric power is generated than dissipated, (3) more electric power is generated than dissipated and the battery is not fully charged, and (4) more electric power is generated than dissipated and the battery is fully charged.

The solar cell does not generate power during an eclipse. Power is generated from direct solar radiation and the albedo, and it is expressed as follows:

$$P_{gen}=\begin{cases}\rho_C\eta_C G_s(A_{pl}+aF_a)l^2 & if\ \ case(2),(3),(4)\\ 0 & if\ \ case(1)\end{cases}. \tag{18}$$

Power is dissipated at the shunt in case (4) in order to prevent overcharge of the battery. For one-nodal analysis,

$$\dot{Q}_{sh\_W}=\begin{cases}P_{gen}-P_W & if\ \ case(4)\\ 0 & if\ \ case(1),(2),(3)\end{cases}. \tag{19}$$

For two-nodal analysis,

$$\dot{Q}_{sh\_I}+\dot{Q}_{sh\_O}=\begin{cases}P_{gen}-P_I-P_O & if\ \ case(4)\\ 0 & if\ \ case(1),(2),(3)\end{cases}. \tag{20}$$

IV. Proposed Thermal Design Procedure

The proposed thermal design procedure for micro- and nano-satellites is as follows. Step 1 is based on concept 1. One-nodal analysis is used to clarify the combinations of optical properties $\alpha_{O\text{-}out}$ and $\varepsilon_{O\text{-}out}$ that keep the satellite within the design temperature range. If the combination is feasible, conduction can be adopted to transfer heat between the inner and outer structures, and the design can skip ahead to step 3. Otherwise, step 2, which is based on concept 2, is performed. Two-nodal analysis is used to obtain the combinations of optical properties for the inner

and outer structures $\alpha_{O\text{-}out}$, $\varepsilon_{O\text{-}out}$, $\varepsilon_{O\text{-}out}$ and ε_I under the condition that the only form of heat transfer between structures is radiation: $\dot{Q}_{I-O_c}=0$ and $\dot{Q}_{O-I_c}=0$. If the combination is feasible, radiation is adopted as the form of heat transfer between the inner and outer structures. If not, the orbit and the component mounted on the micro- and nano-satellite should be reconsidered. In step 3, multi-nodal analysis is performed using the accepted optical properties and form of heat transfer between the inner and outer structures. If all components are within the design temperature range, the thermal design is completed. If not, the emissivity of components outside the design temperature range and the form of heat transfer between the inner plate and those components are modified, and step 3 is performed again.

In the thermal design of satellites, the parameter survey using multi-nodal analysis and measurement of the contact thermal resistance between the structures and components can take a long time. This proposed procedure shortens the thermal design period because the parameter survey is carried out using one- and two-nodal analyses, which have short calculation times, and because the accepted thermal concept is barely influenced by the contact thermal resistance. Because the parameter survey is conducted using one- and two-nodal analyses, the proposed procedure does not obtain the optimum thermal design; however, a reasonable thermal design can be obtained.

V. Verification of Proposed Thermal Design Procedure

A. Satellite Model

The proposed procedure was applied to the Hodoyoshi-1 satellite[9] for verification. Figures 1 and 2 show the schematic and configuration, respectively, of the satellite. Table 1 presents the specifications. The inner structure consisted of two plates. Tables 2-4 list the specifications of the components, structures, and solar cell, respectively. It was difficult to estimate and measure the specific heat of components. Thus, the specific heat of the components was set to 720 J/(kg K). This corresponds to 80% of the specific heat of aluminum alloy A5052, which is 900 J/(kg K).[10] The outer and inner structures were composed of the aluminum honeycomb panels. The conductivity of the honeycomb panel was estimated by referring to Gilmore.[11] The specific heat of the adhesion used for the honeycomb panel is usually not clarified. The specific heat of the honeycomb was set to 714 J/(kg K). This corresponds to 80% of the specific heat of aluminum alloy A3003, which is 893 J/(kg K).[10]

B. Step 1: One-nodal Analysis

Table 5 presents the conditions for one-nodal analysis. The mass, size, and heat dissipation of the satellite model were the same as those listed in Tables 1 and 2. The thermal conductances between structures and between structures and components were set to infinity. The design temperature range differed from that listed in Table 2. When the development period for a thermal design is less than 1 year, a design temperature range is often changed during the thermal design. The design temperature range was changed in order to mimic this situation. Table 6 lists the worst cold and hot conditions. The left side of Fig. 3 shows the node position. The whole satellite was considered to be one node. The average temperature of the whole satellite was calculated at the node. Figure 4 shows the flowchart of the one-nodal analysis. The calculation grid divided the orbit into 8000 parts so that grids would be located at the entrance and exit of the region of eclipse. The absorptivity $\alpha_{O\text{-}out}$ and emissivity $\varepsilon_{O\text{-}out}$ were set at 0.01 intervals.

The one-nodal analysis was carried out under the conditions given in Tables 5 and 6. There was no combination of the solar absorptivity $\alpha_{O\text{-}out}$ and infrared emissivity $\varepsilon_{O\text{-}out}$ for the outside of the outer structure that allowed the satellite to stay within the design temperature range. Thus, the results clarified that concept 1 could not keep the satellite model within the design temperature range.

C. Step 2: Two-nodal Analysis

Table 5 presents the conditions for two-nodal analysis. The mass and heat dissipation of the satellite model were separated into those of the inner and outer structures based on the configurations in Figs.1 and 2 and specifications in Table 2. The size of the satellite model corresponded to that of the Hodoyoshi-1 satellite, as described in Tables 1 and 2. The thermal conductance between the inner and outer structures was set to zero. The shunt was mounted on the outer structure because the one in Table 1 is a sequential shunt. The heat dissipation rate at the shunt in the inner structure $\dot{Q}_{sh\_1}$ is zero in Eq.(20). The design temperature range of the inner structure in two-nodal analysis was the same as in one-nodal analysis. The design temperature range of the outer structure was set wider than that of the inner structure in two-nodal analysis. It is reasonable to assume that the temperature change of the outer structure is larger than the inner structure. The components with the narrower design temperature range were mounted on the inner structure, and the components with the wider design temperature range were mounted on the outer structure. Table 6 lists the worst cold and hot conditions. The right side of Fig. 3 shows the node positions of the two-nodal analysis. The outer and inner structures were each considered to be one node. The average temperatures of the inner

and outer structures were calculated. Figure 5 shows the flowchart of the two-nodal analysis. The calculation grid divided the orbit into 8000 parts so that grids were located on the entrance and exit of the region of eclipse. The absorptivity of the outside of the outer structure $\alpha_{O\text{-}out}$ and emissivity of the outside of the outer structure $\varepsilon_{O\text{-}out}$ were set at 0.01 intervals. The emissivity of the inside of the outer structure $\varepsilon_{O\text{-}in}$ and emissivity of the inner structure ε_I were set at 0.1 intervals. The configuration factor in Eqs. (14) and (15) was calculated by referring to Siegel and Howell.[6]

With the two-nodal analysis, the combinations of solar absorptivity and infrared emissivity of the outside of the outer structure $\alpha_{O\text{-}out}$ and $\varepsilon_{O\text{-}out}$ that would keep the satellite within the design temperature range under the worst hot and cold cases were obtained. The solar absorptivity and infrared emissivity of the radiation area outside the outer structure α_R and ε_R were calculated from Eqs.(6) and (7) by substituting the obtained solar absorptivity and infrared emissivity of the outside of the outer structure $\alpha_{O\text{-}out}$ and $\varepsilon_{O\text{-}out}$ and by substituting the area ratio of the solar cell outside the outer structure for the whole satellite ρ_c, as described in Table 1. Figure 6 shows the calculated combinations of the solar absorptivity and infrared emissivity of the radiation area outside the outer structure α_R and ε_R. The legend shows the number of the combination of $\varepsilon_{O\text{-}in}$ and ε_I for which the satellite stayed within the design temperature for the given α_R and ε_R. Table 7 lists the optical properties of good available surface finishes of aluminum alloy in Japan. The good availability of surface finishes is important to realize the quick development of micro- and nano-satellites. Alodine 1000 was chosen as the surface finish of the outside of the outer structure based on the results in Fig. 6 and Table 7. The solar absorptivity α and infrared emissivity ε of Alodine 1000 are 0.15 and 0.038, respectively. Then, the emissivity of the inside of the outer structure $\varepsilon_{O\text{-}in}$ and emissivity of the inner structure ε_I were considered. Figure 7 shows the maximum and minimum temperatures of the outer and inner structures at α_R = 0.15, ε_R = 0.038. Table 5 shows that the design temperature ranges of the outer and inner structures were from -20 °C to 40 °C, respectively. As shown in Fig. 7, the outer structure had a lower maximum temperature as the emissivities inside the outer structure and of the inner structure were larger. The outer structure had a higher minimum temperature because of these larger emissivities. The graphs of the maximum temperature of the inner structure had almost the same trend when the emissivity inside the outer structure was 0.4 or higher. The maximum temperature of the inner structure drastically decreased when the emissivity of the inner structure was 0.1-0.4. This means that a small change in the emissivity because of a production error or degradation can produce a large change in temperature. The maximum temperature of the inner structure became the minimum when the emissivities of the

inner structure and inside the outer structure became 0.5 and > 0.4, respectively. The maximum temperature of the inner structure gradually increased when the emissivity of the inner structure increased from 0.4 to 0.9. The minimum temperature of the inner structure decreased when the emissivities of the inner structure and inside the outer structure became > 0.3 and > 0.4, respectively, and went below the design temperature limit. $\varepsilon_{O\text{-}in}$ and ε_I should be set to 0.4 to keep the components within the design temperature range and prevent large changes in temperature because of production errors or degradation. The normal emissivity of UPILEX 012R-TANN is 0.42. The design temperature ranges of the outer and inner structures were changed to -20 °C to 35 °C and 5 °C to 35 °C, respectively. As shown in Fig. 7, the maximum temperature of the outer structure was beyond the upper limit of the new design temperature range. The maximum temperature of the outer structure was lower when the emissivities inside the outer structure and of the inner structure were larger. Black alumite was chosen as the surface finish inside the outer structure and of the inner structure based on the new design temperature range.

D. Step 3: Multi-nodal Analysis

The satellite model for multi-nodal analysis is shown in Figs. 1 and 2 and described Table 2. The demands from the other subsystems were applied to this satellite model. The surface finish of the battery was Alodine 1200. The surface finishes on the inside and outside of the opening of the star tracker were black alumite and Alodine 1000, respectively. The surface finishes on the outside and inside of the outer structure of the sun sensor were black alumite and Alodine 1200, respectively. Figure 8 shows the schematic of the mission camera. The surface finish inside the opening of the mission camera was black alumite. The surface finish outside the hood of the mission camera was Alodine 1000. The surface finish on the leg of the mission camera was black alumite. MLI was set for the outside parts of the mission camera except for the hood and legs. The effective emissivity of MLI and the optical properties of the mirror and lens are listed in Table 8. The optical properties of the radiative areas outside of the outer structure, inside the outer structure, of the inner structure, and of the components excluding the battery, star tracker, sun sensor, and mission camera were set to the optical properties obtained in the two-nodal analysis of step 2: α_R = 0.15, ε_R = 0.038, $\varepsilon_{O\text{-}in}$ = 0.88, and ε_I = 0.88. In order to realize the conductive heat transfer in two-nodal analysis, thermal conductive sheets were inserted between plates of the outer structure, between plates of the inner structure, and between plates and components. Insulators with a thickness of 1.0 mm were set between the outer and inner structures. The conductivities of the thermal conductive sheet and insulators are presented in Table.9.

Table 10 presents the number of nodes in the multi-nodal analysis. The design temperature range of the multi-

nodal analysis is presented in Table 2. The worst cold and hot conditions are listed in Table 11. Production errors and degradation of the surface finish were considered along with the worst cold and hot conditions used in the one- and two-nodal analyses, as described in Table 6. The heat transfer rates of radiation from node i to node j and vice versa are respectively expressed as follows:

$$\dot{Q}_{i-j\,r}=\frac{\sigma(T_i^{\,4}-T_j^{\,4})}{(1/\varepsilon_j-1)/A_j+(1/\varepsilon_i-1)/A_i+1/(A_iF_{i-j})}\,, \tag{21}$$

$$\dot{Q}_{j-i\,r}=\frac{\sigma(T_j^{\,4}-T_i^{\,4})}{(1/\varepsilon_j-1)/A_j+(1/\varepsilon_i-1)/A_i+1/(A_jF_{j-i})}\,. \tag{22}$$

It is difficult to mathematically calculate $F_{i\text{-}j}$ and $F_{j\text{-}i}$ in multi-nodal analysis because the shape and configuration of nodes i and j are complicated. $F_{i\text{-}j}$ and $F_{j\text{-}i}$ were numerically calculated using the Monte Carlo method. In this study, SINDA/FLUINT version 4.8 was used as a solver, and Thermal Desktop version 4.8 was used as a pre-processing and post-processing tool.

Table 12 presents the temperature of the components obtained by the multi-nodal analysis. All of the components except for the battery and star tracker stayed within the design temperature range. The battery went below and above the temperature limits in the worst cases. The star tracker exceeded the higher temperature limit.

The satellite model used in the multi-nodal analysis was modified as follows: 1) The conductive control material between the Earth-pointing surface (-Z) and the inner structure was changed from an insulator to a thermal conductive sheet. 2) The surface finish outside the hood of the star tracker was changed from Alodine 1000 to black alumite. 3) The conductive thermal material between the battery and inner structure was changed from a thermal conductive sheet to an insulator. 4) The surface finish outside the +Z plate of the outer structure was changed from black alumite to white alumite. Table 13 presents the temperatures of the components after these modifications. The temperatures of all of the components were successfully lowered. All of the components except for the battery stayed within the design temperature range. The battery in the worst cold case was below the lower limit of the design temperature range. Setting a heater on the battery can increase the temperature. Adding a heater of 2.9 W to the battery caused the temperature range in the worst cold case to become 4.1-8.3 °C. Thus, a heater of 5 W should keep the battery within the design temperature range.

This thermal design was completed in ten months; it included the development of one- and two-analysis codes

and a satellite model for multi-nodal analysis. The solar contact, Earth infrared radiation and albedo in the worst cases are severe conditions that only occur for 3 h in 1 year. The degradation of optical properties and the shift of LTDN were also considered for the worst cases. The obtained thermal design has high robustness. Therefore, the proposed procedure allows the thermal design of micro- and nano-satelltes to be completed quickly and with sufficient reliability.

The results of the two- and multi-nodal analyses were compared. Figures 9 and 10 compare the results for the outer structure in the worst hot and cold cases, respectively. The optical properties obtained in the two-nodal analysis (α_R = 0.15, ε_R = 0.038, $\varepsilon_{O\text{-}in}$ = 0.88 and ε_I = 0.88) were applied to the satellite model used in the multi-nodal analysis except for the solar cell and the mirror and lens of the mission camera. The worst hot and cold cases in Table 6 were used to compare the two- and multi-nodal analysis results. The two analyses agreed in the trend of the temperature. In the worst hot case, the two-nodal analysis produced an average peak temperature that was about 4 °C lower than that of the multi-nodal analysis. In the worst cold case, the two-nodal analysis produced an average peak temperature that was about 6 °C lower than that of the multi-nodal analysis. Figures 11 and 12 compare the heating rates absorbed at the solar cell of the two analysis methods in the worst hot and cold cases, respectively. The two-nodal analysis produce lower heating rates than the multi-nodal analysis in both worst cases. The average area ratio of the solar cell outside the outer structure was used to calculate the heating rate absorbed at the solar cell in the two-nodal analysis. The area ratio of the solar cell in each plate consisting of the outer structure was used in the multi-nodal analysis. Solar radiation is not equally incident equally on plates of the outer structure in the case of Earth-pointing satellites. This caused the difference in the heating rate absorbed at the solar cell. The calculated heating rate absorbed at solar cells in two-nodal analysis was revised to be calculated at each plate.

Figures 13 and 14 compare the calculated temperatures of the multi-nodal and revised two-nodal analyses. The differences were smaller than the differences between the temperatures shown in Figs. 11 and 12. The temperature differences between the revised two-nodal and multi-nodal analyses were 2 and 3 °C in the worst hot and cold cases, respectively. Thus, two-nodal analysis that considers the heating rate absorbed at each plate of the outer structure is effective at predicting the temperature of micro and nano satellites. Figures 15 and 16 compare the results of the original two-nodal analysis, revised two-nodal analysis, and multi-nodal analysis for the inner structure in the worst hot and cold cases, respectively. The temperature trends of the two- and multi-nodal analyses did not correspond in the two cases. Table 14 presents the mass and heat generation rate of the +Y side and -Y side plates comprising the

inner structure. The two-nodal analysis used the total mass in Table 14. The multi-nodal analysis utilized the mass of each plate. The difference in heat capacity caused the difference in temperature change. Two-nodal analysis was carried out where the mass of the inner structure equaled the mass of the +Y side inner plate (3.2 kg). Figures 17 and 18 compare the temperature histories of the inner structure under the worst hot and cold cases using multi- and two-nodal analyses. For the multi-nodal analysis, the mass of the -Y side plate of the inner structure was removed so that the mass of the model was the same as that of two-nodal analysis. The trends of the average temperature for the two analysis methods corresponded. Thus, the mass of each plate should be considered in two-nodal analysis when the inner structure has several plates and one has a greatly different mass from the others.

The conductive heat transfer between the inner and outer structures was considered to be 0 in the two-nodal analysis. Conductive heat transfer between the inner and outer structures was considered in the multi-nodal analysis. As shown in Figs. 13, 14, 17 and 18, the difference in temperatures between the two- and multi-nodal analyses was small. Thus, assuming that the conductive heat transfer between the inner and outer structures in two-nodal analysis is 0 is valid for the thermal design of micro- and nano-satellites. Concept 2 was realized by using an insulator with a thickness of 1 mm or more and conductive sheets.

VI. Conclusion

The proposed procedure can be used to complete the thermal design of micro- and nano-satellites in about 1 year. The procedure is based on two concepts to keep the components within the design temperature range: (1) reduce the temperature change by exploiting the thermal capacity of the entire satelite and (2) reduce the temperature change of the inner structure, where the most temperature-sensitive components are mounted. One- and two-nodal analyses are carried out for a parameter survey of the optical properties that will keep components within the design temperature range. One-nodal analysis is used to design the satellite under concept 1. Two-nodal analysis, where the outer and inner structures are each considered to be a node, is used to design the satellite under concept 2. Finally, multi-nodal analysis is carried out for detailed design using the optical properties obtained by the previous analyses. This thermal design procedure was applied to the Hodoyoshi-1 satellite. The thermal design was completed in ten months. The proposed procedure was demonstrated to help realize a quick and effective thermal design of micro- and nano-satellites.

Acknowledgments

This research was supported by a grant from the Japan Society for the Promotion of Science (JSPS) through the "Funding Program for World-Leading Innovative R&D on Science and Technology (FIRST Program)" initiated by the Council for Science and Technology Policy (CSTP).

References

[1]Nakasuka, S., "New Paradigm of Space Development and Utilization opened by Nano-satellites," *1st Nano-Satellite Symposium*, Oct. 10, 2010, [online], URL: http://www.nanosat.jp/1st/information_e.html.

[2]Weeren, H., Brake, H. J. M., Holl, G., Hamann, R. J. and Price, S., "Thermal Aspects of Satellite Downscaling," *Journal of Thermophysics and Heat Transfer*, 23, 3, 2009, pp. 592-600.

[3]Ramamurthi, K., Kumar, S. S. and Abilash, P. M., "Thermal Contact Conductance of Molybdenum-Sulphide-Coated Joints at Low Temperature," *Journal of Thermophysics and Heat Transfer*, 21, 4, 2007, pp. 811-813.

[4]Bahrami, M., Culham, J. R., Yovanovich, M. M. and Schneider, G. E., "Thermal Contact Resistance of Nonconforming Rough Surfaces, Part 2: Thermal Model," *Journal of Thermophysics and Heat Transfer*, 18, 2, 2004, pp. 218-227.

[5]Milanez, F. H., Yovanovich, M. M. and Mantelli, M. B. H., "Thermal Contact Conductance at Low Pressures," *Journal of Thermophysics and Heat Transfer*, 18, 1, 2004, pp. 37-44.

[6]Siegel, R. and Howell, J. R., *Thermal Radiation Heat Transfer,* 2nd ed., Hemisphere Publishing Corporation, New York, 1981, p.829.

[7]Bannister, J. C., *Radiation Geometry Factor between the Earth and a Satellite*, NASA TND-2750, 1965.

[8]Totani, T., Ogawa, H., Inoue, R., Wakita, M. and Nagata, H., "Thermal Design of Nano and Micro Satellites on Sun-synchronous Orbits," *The 28th International Symposium on Space Technology and Science*, 2011-f-34, The Japan Society for Aeronautical and Space Sciences, Ginowan, 2011.

[9]Miyashita, N., Nakamura, Y., Nakasuka, S., Iwasaki, A., Totani, T., Sahara, H., Enoguchi, A., Takeyama, Y., Hayakawa, Y. and Yamaguchi, K.: Current Status and Perspective of Hodoyoshi-1 Satellite, Proceedings of 55th Space Sciences and Technology Conference, 2011, JSASS-2011-4436, in Japanese.

[10]Japan Aluminum Association, *Characteristics Database of Aluminum Materials* [online database], URL: http://metal.matdb.jp/JAA-DB/ [cited 4 September 2013].

[11]Gilmore, D. G. (ed.), *Spacecraft thermal control handbook*, 2nd ed., Vol.1, the Aerospace Press, El Segundo, CA, 2002, pp. 814-818.

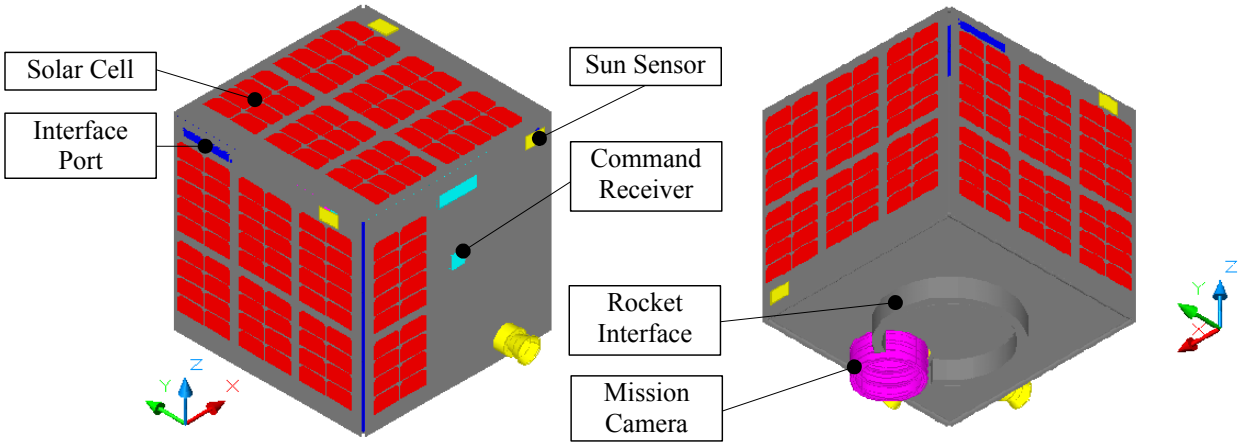

Figure 1. Schematic of satellite model.

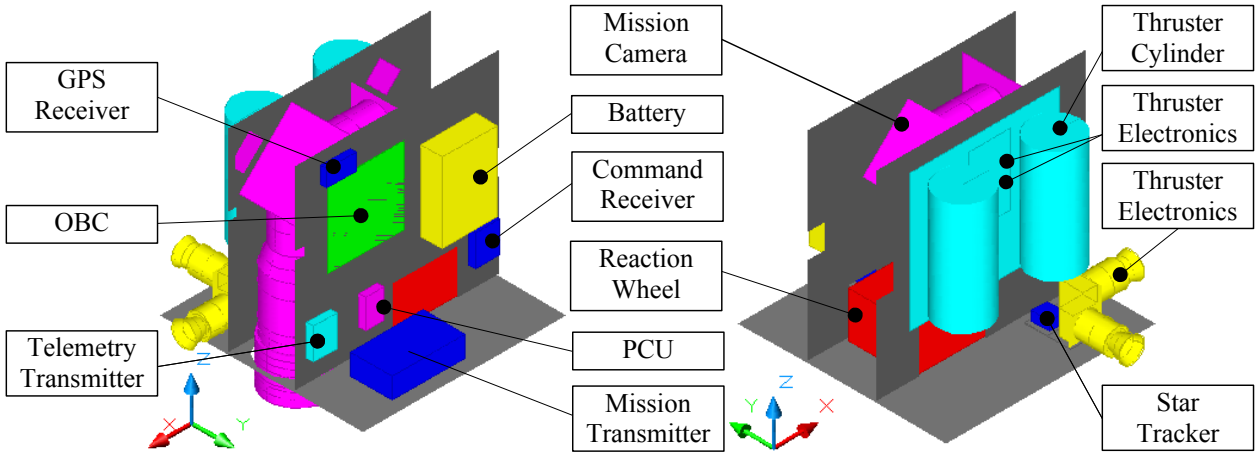

Figure 2. Configuration of components and inner structure.

Table 1. Specifications of Hodoyoshi-1 satellite.

Mass, kg	49.6
Size, m^3	0.5 × 0.5 × 0.5
Inner structure	2 plates
Orbit	Sun-synchronous and circular
Altitude, km	500
Local time descending node	11:00 AM
Attitude	Earth pointing
Power generation	Ultra triple junction solar cell
Setting method of solar cell	Body mount
Area ratio of solar cell on outside of outer structure	-X: 0.577, +X: 0.579, -Y: 0.196, +Y: 0.572, -Z: 0.000, +Z: 0.573 Whole satellite: 0.417
Battery	Lithium-ion battery
Shunt	Sequential shunt

Table 2. Specifications of components.

Components	Mass, kg	Specific heat, J/(kg K)	Conductivity, W/(m K)	Dissipation, W	Design temperature range, °C
On-board computer	0.30	720	137	5.00	-25 to 55
GPS receiver	0.068	720	137	0.13	-25 to 65
Telemetry transmitter	0.13	720	137	0.00	-25 to 80
Mission transmitter	1.00	720	137	0.00	-25 to 75
Command receiver	0.037	720	137	0.20	-25 to 80
Battery	1.68	720	137	charge: 0.08 discharge: 0.72	5 to 35
Gyro sensor	0.0476	720	137	1.50	-35 to 80
Sun sensor	0.0095×5	720	137	0.15×5	-35 to 80
Magnetic sensor	0.054	720	137	0.06	-40 to 70
Magnetic torquer	0.71	720	137	3.56	-35 to 80
Star tracker	0.94	720	137	2.50	-15 to 35
Reaction wheel	4.56	720	137	1.65	-15 to 45
Thruster	12.2	720	137	0.00	-15 to 125
Mission camera	14.0	710 to 896	1.67 to 167	0.00	All parts of mission camera is within an arbitrary temperature ± 15 °C.

Table 3. Specifications of structures.

Structures	Mass, kg	Specific heat, J/(kg K)	Conductivity, W/(m K)
-X	1.06	714	13.84
+X	1.06	714	13.84
-Y	1.05	714	13.84
+Y	1.07	714	13.84
-Z	1.08	714	13.84
+Z	1.08	714	13.84
Columns (4 parts)	2.06	720	140
-Y inner plate	0.93	714	13.84
+Y inner plate	0.93	714	13.84

Table 4. Specifications of solar cell.

Size, mm × mm	39.6 × 69.0
Density, mg/cm^2	84
Efficiency, %	28.3
Solar absorptivity	0.92
Infrared emissivity	0.85

Table 5. Conditions for one- and two-nodal analyses.

	One-nodal analysis	Two-nodal analysis
Mass, kg	49.6	Outer Structure: 20.7 Inner Structure: 28.9
Size, m^3	0.5 × 0.5 × 0.5	0.5 × 0.5 × 0.5
Specific heat, J/(kg·K)	720	720
Thickness of inner structural panel (aluminum honeycomb), m	-	0.01
Thickness of outer structural panel (aluminum honeycomb), m	-	0.01
Inner structure	-	Two plates
Distance between inner plates, m	-	0.16
Thermal conductance between inner and outer structure, W/(K)	∞	0
Heat dissipation, W	15.35	Outer Structure: 10.02 Inner Structure: 5.33
Position of shunt	-	Outer structure
Design temperature range, °C	10 to 40	Outer structure:-20 to 40 Inner structure:10 to 40

Table 6. Worst cold and hot conditions in one-and two-nodal analyses.

	Worst Cold	Worst Hot
Solar contact, W/m^2	1309	1414
Earth infrared radiation, W/m^2	189	261
Albedo factor	0.2	0.4
Initial temperature, K	10	25
Initial position for calculation	Entrance of eclipse	Exit of eclipse

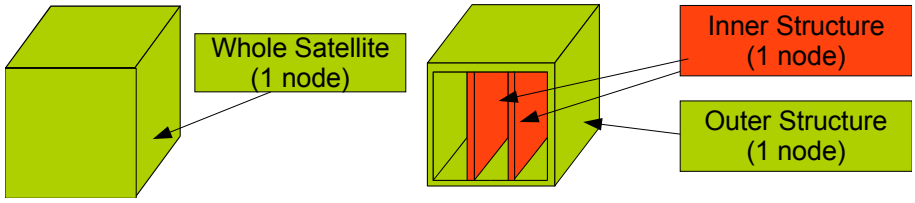

Figure 3. Position of node in one- and two-nodal analyses.

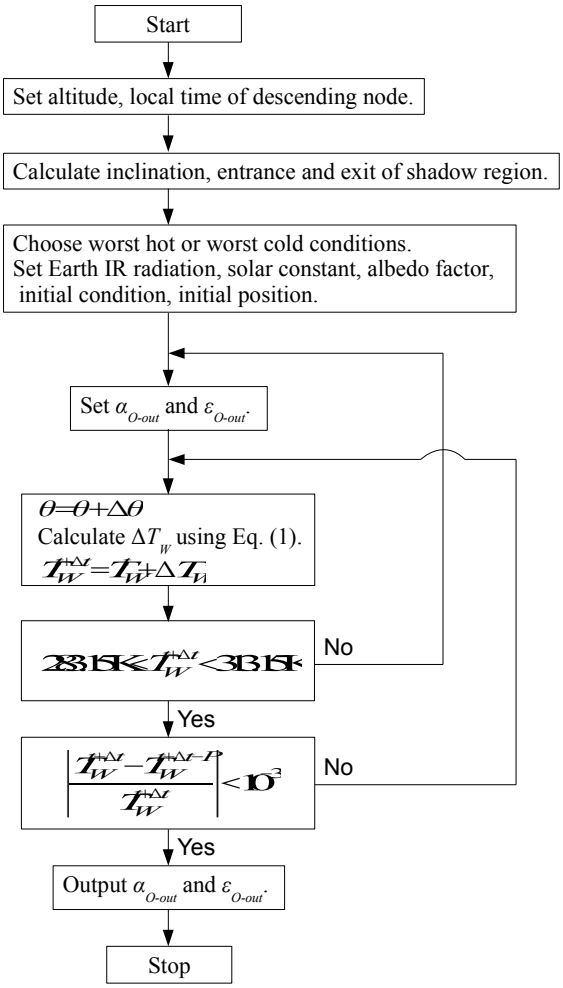

Figure 4. Flowchart of one-nodal analysis.

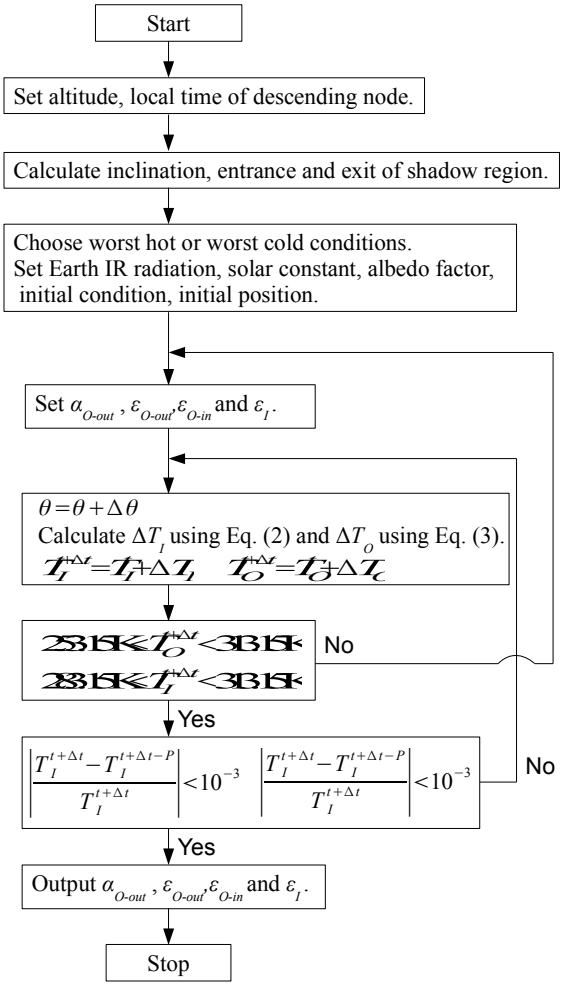

Figure 5. Flowchart of two-nodal analysis.

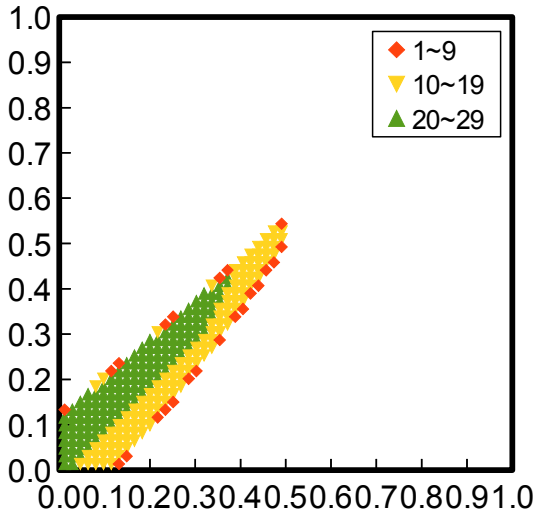

Figure 6. Combinations of α_R and ε_R when satellite temperature stays within design temperature range under worst hot and cold cases.

Table 7. Optical properties of surface finishes.

	α	ε	α/ε
Alodine 1000	0.15	0.038	3.95
Alodine 1200	0.39	0.068	5.74
White alumite	0.24	0.76	0.32
Black alumite	0.68	0.88	0.77

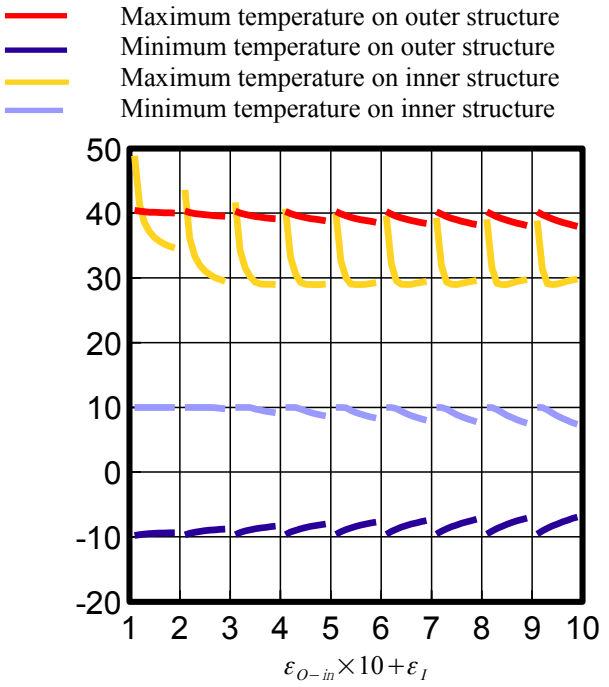

Figure 7. Maximum and minimum temperature on outer and inner structure: $\alpha_R = 0.15$, $\varepsilon_R = 0.038$.

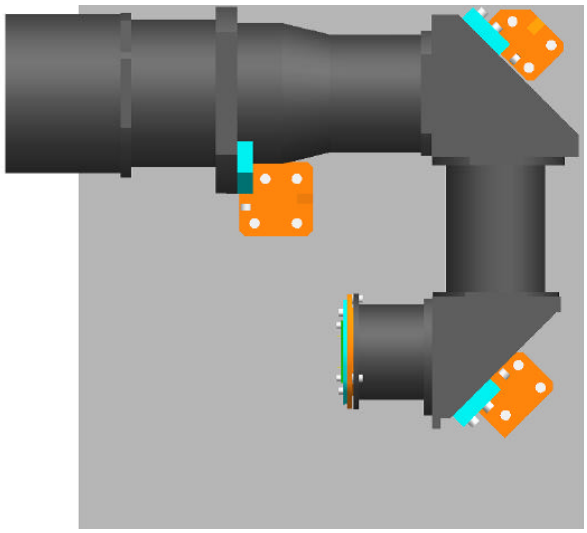

Figure 8. Schematic of mission camera.

Table 8. Optical properties of surface finishes of mission camera.

	α	ε	α/ε
Black Alumite	0.76	0.82	0.93
MLI	-	0.008	-
Lens	0.00	1.00	0.00
Mirror	0.00	1.00	0.00

Table 9. Conductivity of insulator and thermal conductive sheet.

	Conductivity
Glass epoxy	0.471 W/(m·K)
DENKA BFG20	4.1 W/(m·K)

Table 10. Number of nodes in multi-nodal analysis.

On-board computer	1	-X	24
GPS receiver	1	+X	35
Telemetry transmitter	1	-Y	44
Mission transmitter	1	+Y	20
Command receiver	1	-Z	30
Battery	1	+Z	22
Gyro sensor	3	Inner plates	56
Sun sensor	5	Columns	12
Magnetic sensor	1	Solar cells	26
Magnetic torquers	15	Output port	11
Star tracker	30	Thruster	6
Reaction wheel	1	Mission camera	53
		Total	400

Table 11. Worst cold and hot conditions in multi-nodal analysis.

	Worst Cold	Worst Hot
Solar contact, W/m^2	1309	1414
Earth infrared radiation, W/m^2	189	261
Albedo factor	0.2	0.4
Initial temperature, K	10	25
Initial position for calculation	Entrance of eclipse	Exit of eclipse
Shift of local time descending node (LTDN)	+1 h LTDN: 12:00	-1 h LTDN: 10:00
Production error	Alodine 1000 ε: 0.038 → 0.06	Alodine 1000 α: 0.15 → 0.20
Degradation	-	White alumite α: 0.24 → 0.68 ε: 0.76 → 0.88

Table 12. Temperature of components.

Components	Worst cold case, °C	Worst hot case, °C
On-board computer	-0.6 to 11.3	24.3 to 41.5
GPS receiver	-4.6 to 11.1	19.3 to 41.5
Telemetry transmitter	-3.3 to 10.7	21.1 to 41.2
Mission transmitter	-7.0 to 11.7	17.1 to 42.7
Command receiver	-3.6 to 11.8	20.7 to 42.0
Battery	-0.7 to 11.3	24.2 to 41.5
Gyro sensor	-7.0 to 11.6	16.9 to 42.3
Sun sensor	-9.2 to 13.8	14.0 to 44.3
Magnetic sensor	-9.2 to 12.2	14.0 to 42.8
Magnetic torquer	-9.1 to 13.5	14.1 to 44.1
Star tracker	-7.2 to 11.9	16.5 to 41.8
Reaction wheel	-6.7 - 11.8	17.6 to 42.6
Thruster	0.78 - 4.8	27.5 to 33.8

Table 13. Temperature of components.

Components	Worst cold case, °C	Worst hot case, °C
On-board computer	-7.6 to 6.6	17.5 to 37.5
GPS receiver	-12.5 to 7.7	10.9 to 39.1
Telemetry transmitter	-10.0 to 6.3	14.3 to 38.3
Mission transmitter	-8.2 to 6.3	16.8 to 37.3
Command receiver	-8.8 to 6.7	16.1 -to 37.9
Battery	-2.4 to 2.0	24.8 to 31.0
Gyro sensor	-8.7 to 6.4	16.1 to 37.3
Sun sensor	-17.3 to 11.0	4.8 to 42.9
Magnetic sensor	-16.9 to 9.3	5.4 to 41.0
Magnetic torquer	-17.1 to 10.7	5.1 to 42.8
Star tracker	-9.9 to 6.8	14.3 to 35.0
Reaction wheel	-8.2 to 6.3	16.8 to 37.3
Thruster	-4.4 to 0.2	22.3 to 29.7

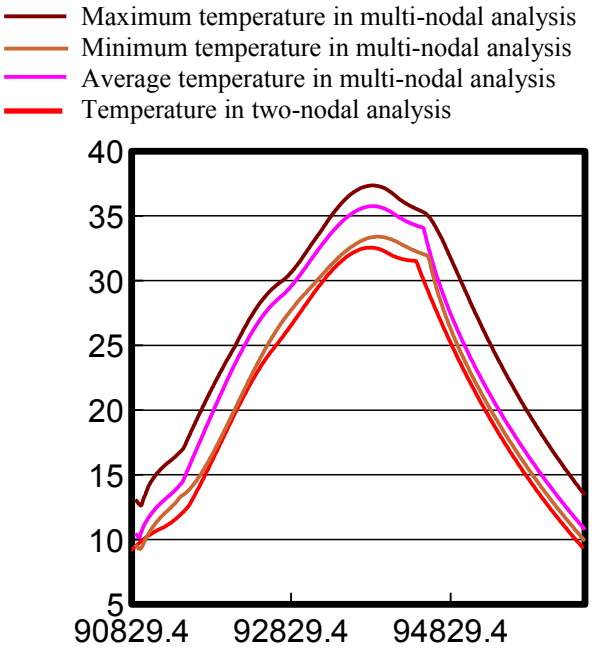

Figure 9. Comparison of temperature history at outer structure under worst hot case between two- and multi-nodal analyses.

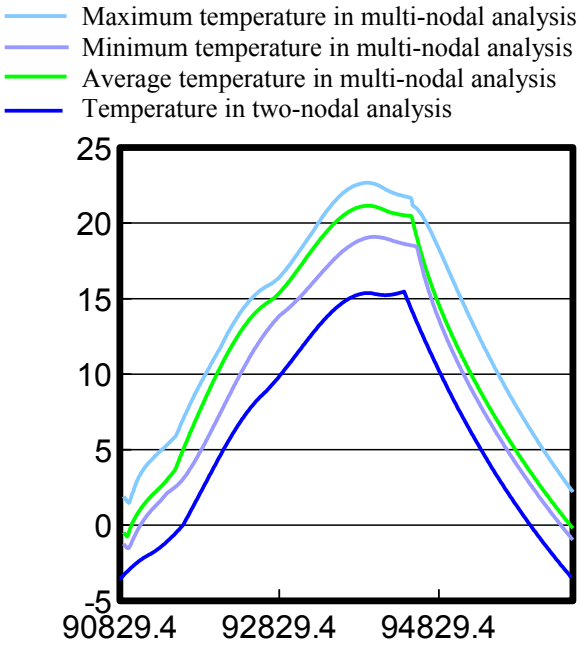

Figure 10. Comparison of temperature history at outer structure under worst cold case between two- and multi-nodal analyses.

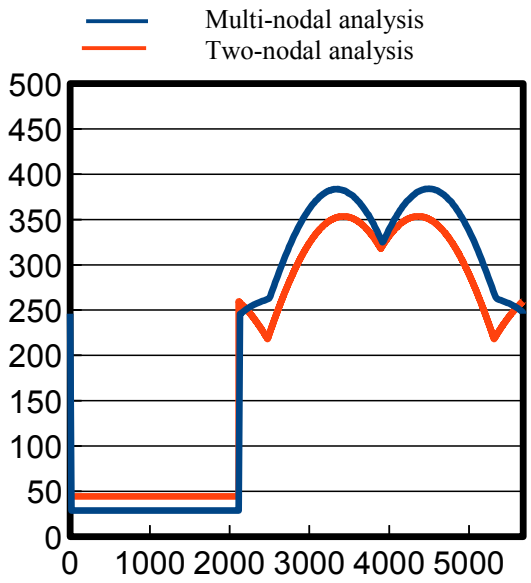

Figure 11. Comparison of absorbed heating rate history at solar cell under worst hot case between two- and multi-nodal analysis.

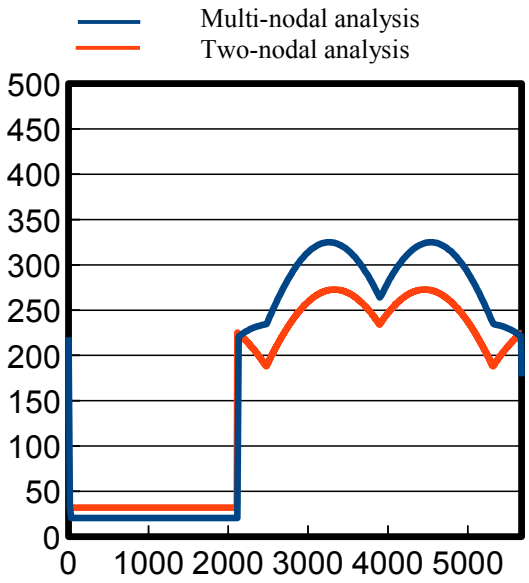

Figure 12. Comparison of absorbed heating rate history at solar cell under worst cold case between two- and multi-nodal analysis.

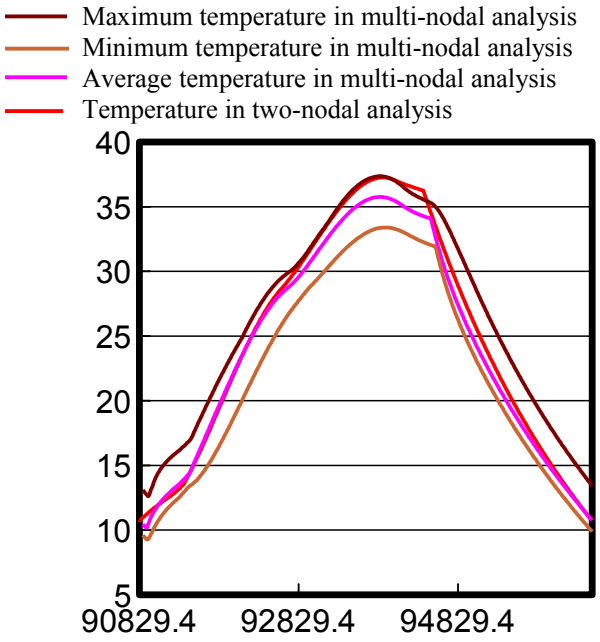

Figure 13. Comparison of temperature history at outer structure under worst hot case between two-nodal analysis with revised absorption at solar cells and multi-nodal analysis.

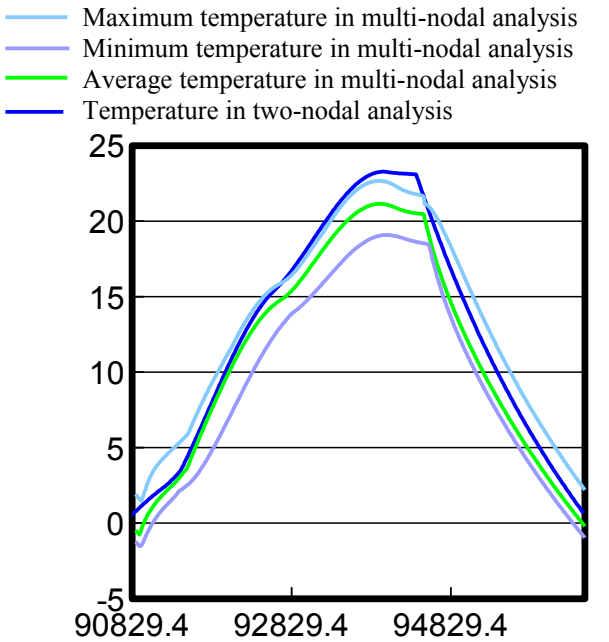

Figure 14. Comparison of temperature history at outer structure under worst cold case between two-nodal analysis with revised absorption at solar cells and multi-nodal analysis.

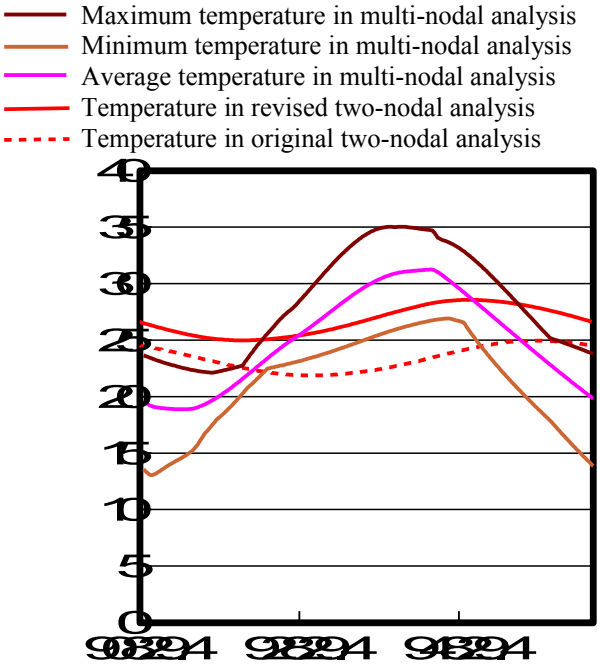

Figure 15. Comparison of temperature history at inner structure under worst hot case between two- and multi-nodal analyses.

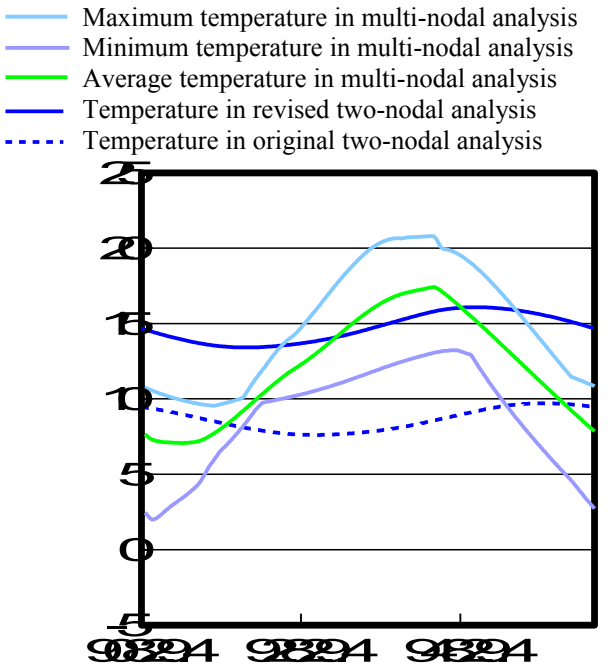

Figure 16. Comparison of temperature history at inner structure under worst cold case between two- and multi-nodal analyses.

Table 14. Mass and heat generation rate of inner structure.

	Mass	Heat generation rate
Inner plate of +Y side	3.2 kg	5.33 W
Inner plate of -Y side	25.7 kg	0 W
Total	28.9 kg	5.33 W

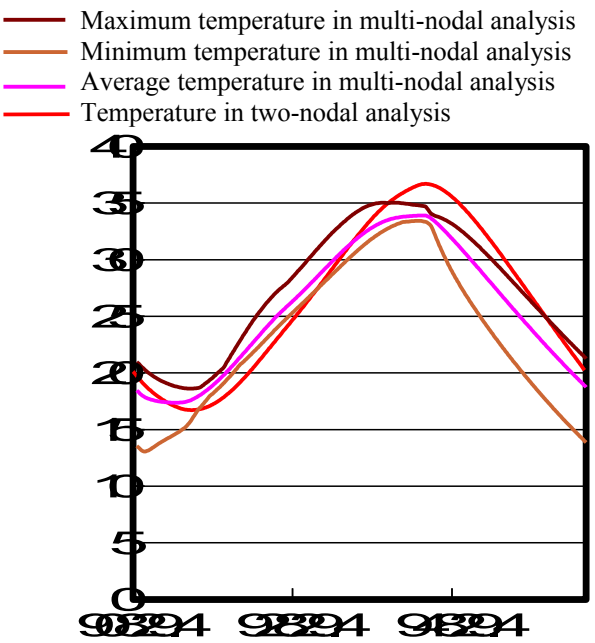

Figure 17. Comparison of temperature history at inner structure under worst hot case between two- and multi-nodal analyses with mass of inner structure of 3.2 kg.

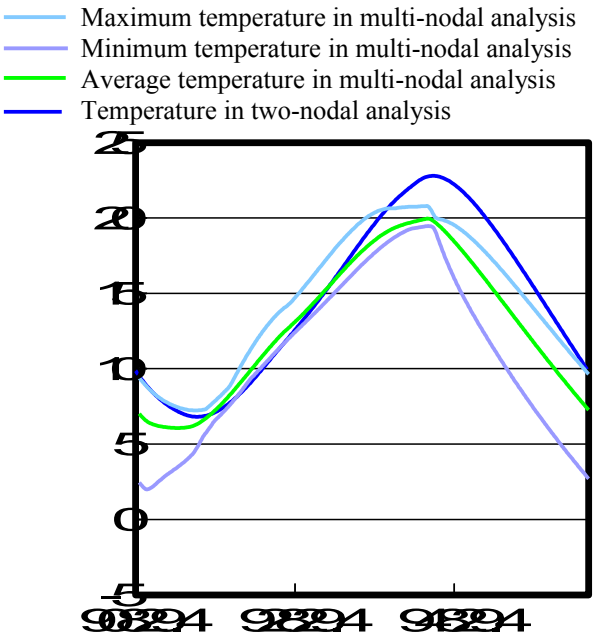

Figure 18. Comparison of temperature history at inner structure under worst cold case between two- and multi-nodal analyses with mass of inner structure of 3.2 kg.